J Physiol 594.24 (2016) pp 7197–7213

The Journal of Physiology

TECHNIQUES FOR PHYSIOLOGY

Development of a high-throughput method for real-time assessment of cellular metabolism in intact long skeletal muscle fibre bundles

Rui Li[1], Frederik J. Steyn[1,2], Michael B. Stout[3], Kevin Lee[1], Tanya R. Cully[1], Juan C. Calderón[4] and Shyuan T. Ngo[1,2,5,6]

[1] *School of Biomedical Sciences, University of Queensland, Brisbane, Australia*
[2] *University of Queensland Centre for Clinical Research, Brisbane, Australia*
[3] *Robert and Arlene Kogod Center on Aging, Mayo Clinic, Rochester, MN, USA*
[4] *Department of Physiology and Biochemistry, Physiology and Biochemistry Research Group-PHYSIS, Faculty of Medicine, University of Antioquia, Medellín, Colombia*
[5] *Queensland Brain Institute, University of Queensland, Brisbane, Australia*
[6] *Department of Neurology, Royal Brisbane and Women's Hospital, Brisbane, Australia*

Key points

- We developed a method that allows for real-time assessment of cellular metabolism in isolated, intact long skeletal muscle fibre bundles from adult mice.
- This method can be used to study changes in mitochondrial function and fuel utilisation in live skeletal muscle fibre bundles.
- Our method enables flexibility in experimental design and high-throughput assessment of mitochondrial parameters in isolated skeletal muscle fibre bundles.
- Extensor digitorum longus (EDL) fibre bundles obtained from chronic high-fat diet fed mice had lower basal oxygen consumption under FCCP-induced maximal respiration, when compared to control chow-fed mice.
- EDL fibre bundles obtained from chronic high-fat diet fed mice had enhanced mitochondrial oxidation capacity under FCCP-induced maximal respiration, when compared to control chow-fed mice.

Abstract Metabolic dysfunction in skeletal muscle contributes to the aetiology and development of muscle diseases and metabolic diseases. As such, assessment of skeletal muscle cellular bioenergetics provides a powerful means to understand the role of skeletal muscle metabolism in disease and to identify possible therapeutic targets. Here, we developed a method that allows for the real-time assessment of cellular respiration in intact skeletal muscle fibre bundles obtained from the extensor digitorum longus (EDL) muscle of adult mice. Using this method, we assessed the contribution of ATP turnover and proton leak to basal mitochondrial oxygen consumption rate (OCR). Our data demonstrate that the mitochondria in EDL fibres are loosely coupled. Moreover, in the presence of carbonyl cyanide-*p*-trifluoromethoxyphenylhydrazone (FCCP), we show that palmitate exposure induced comparable peak OCR and higher total OCR in EDL fibre bundles when compared to pyruvate exposure, suggesting that fatty acids might be a more sustainable fuel source for skeletal muscle when mitochondria are driven to maximal respiration. Application of this method to EDL fibre bundles obtained from chronic high-fat diet fed mice revealed lower basal OCR and enhanced mitochondrial oxidation capacity in the presence of FCCP when compared to the chow-diet fed control mice. By using a 96-well microplate format, our method provides a flexible and efficient platform to investigate mitochondrial parameters of intact skeletal muscle fibres obtained from adult mice.

DOI: 10.1113/JP272988

(Received 22 June 2016; accepted after revision 7 September 2016; first published online 13 September 2016)
Corresponding author S. Ngo: School of Biomedical Sciences, University of Queensland, St Lucia, QLD 4072, Australia. Email: s.ngo@uq.edu.au

Abbreviations AUC, area under the curve; DMEM, Dulbecco's modified Eagle's medium; ECAR, extracellular acidification rate; ECM, extracellular matrix; EDL, extensor digitorum longus; ETC, electron transport chain; FBS, fetal bovine serum; FCCP, carbonyl cyanide-*p*-trifluoromethoxyphenylhydrazone; FDB, flexor digitorum brevis; FFM, fat free mass; FM, fat mass; HFD, high-fat diet; OCR, oxygen consumption rate.

Introduction

Skeletal muscle is one of the major organs that determines basal energy expenditure (Zurlo *et al.* 1990), and it is responsible for 75–95% of insulin-mediated glucose uptake (Baron *et al.* 1988; DeFronzo, 1988). Insulin resistance, along with dysregulation of glucose and fat metabolism in skeletal muscle, is closely associated with diabetes, obesity and other chronic metabolic conditions (Phielix & Mensink, 2008; Wells *et al.* 2008). Recent studies have also linked metabolic dysfunction in skeletal muscle with motor pathologies seen in neurodegenerative diseases including Alzheimer's disease (Schuh *et al.* 2014), Huntington's disease (Ciammola *et al.* 2011) and amyotrophic lateral sclerosis (Palamiuc *et al.* 2015). Moreover, skeletal muscle is a regulator of its own metabolism and that of other tissues through the release and action of myokines (Ahima & Park, 2015). As such, analyses of cellular bioenergetics in skeletal muscle presents an opportunity to better understand muscle metabolism and the impact of disease on muscle function.

Current approaches that assess serum levels of muscle metabolic enzymes to clinically monitor muscle injury and neuromuscular disease (Pearson, 1957; Pearce *et al.* 1964; Zhang *et al.* 2012*b*) are usually restricted to fixed time point measurements. While it is also common to measure mitochondrial enzymes as a proxy of mitochondrial function (Spinazzi *et al.* 2012; Van Bergen *et al.* 2014), the dynamic nature of whole body metabolism and cellular metabolism renders it difficult to accurately determine the content, or activity of enzymes as a means to depict the true metabolic networks (Thorburn, 2000; Chen *et al.* 2011). In this regard, quantitative assessment of metabolic flux using stable isotopes such as ^{3}H and ^{13}C allows elucidation of the flux of elements through metabolic pathways (Gollnick *et al.* 1985; Chokkathukalam *et al.* 2014). However, isotopic labelling can be limited by costly reagents, altered molecular behaviours after labelling, and potential radioactive hazards (Shan *et al.* 2000; Bueschl *et al.* 2013).

Following the development of the Clark electrode (Clark, 1956), many oxygen electrode systems have been developed to measure oxygen tension in biological samples (Clark & Sachs, 1968; Grassi *et al.* 1996; Jung *et al.* 1999; Pasarica *et al.* 2009). More recently, the Seahorse XF Extracellular Flux Analyser has been introduced as a complementary method to allow for the assessment of mitochondrial parameters (Wu *et al.* 2007; Ferrick *et al.* 2008; Zhang *et al.* 2012*a*). The microplate format equipped with fluorescence-based biosensors allows the simultaneous assessment of mitochondrial respiration and glycolysis in cells (Ferrick *et al.* 2008). Previous studies have successfully used this technology to assess bioenergetics in live tissues such as zebrafish embryos (Stackley *et al.* 2011) and rat brain slices (Fried *et al.* 2014).

More recently, Schuh and colleagues developed a method to assess mitochondrial respiration in intact short muscle fibres in a XF24 microplate format (Schuh *et al.* 2012). The use of intact muscle fibres for assessing mitochondrial function circumvents some limitations associated with the disruption of mitochondrial structure and function that can occur during the preparation of isolated mitochondria (Picard *et al.* 2010; Picard *et al.* 2011). Despite these advances, the approach is restricted to a lower throughput 24-well plate format and the use of short skeletal muscle fibres (e.g. flexor digitorum brevis; FDB). In this regard, variable mitochondrial content (Isaeva *et al.* 2005) and differential glucose uptake ability (Mackrell & Cartee, 2012) between short and long skeletal muscle fibres are indicative of differing cellular bioenergetics between the muscle fibre types. Given that the extensor digitorum longus (EDL) is commonly used to study skeletal muscle function, we have developed a method (summarised in Fig. 1*A* and 1*B*) that allows for the real-time assessment of cellular metabolism in intact long skeletal muscle fibres in a higher throughput Seahorse XF^{e}96-well microplate format.

Methods

Ethical approval and animal welfare

All experimental procedures were approved by the University of Queensland Animal Ethics Committee under the ethics numbers SBMS/562/12/NHMRC/MNDRIA and SBMS/520/15/NHMRC/MNDRIA. Experiments complied with policies and regulations regarding animal experimentation (Drummond, 2009), and were conducted in accordance with the Queensland Government Animal Care and Protection Act 2001, associated Animal Care and Protection Regulations (2002 and 2008), and the *Australian Code of Practice for the Care*

and Use of Animals for Scientific Purposes, 7th Edition (National Health and Medical Research Council, 2004). All authors understand the ethical principles under which *The Journal of Physiology* operates.

Mice

Male C57BL/6J mice (15–20 weeks of age) were used for the method optimisation ($n = 4$), the mitochondrial stress assay ($n = 4$) and the substrate utilisation assay

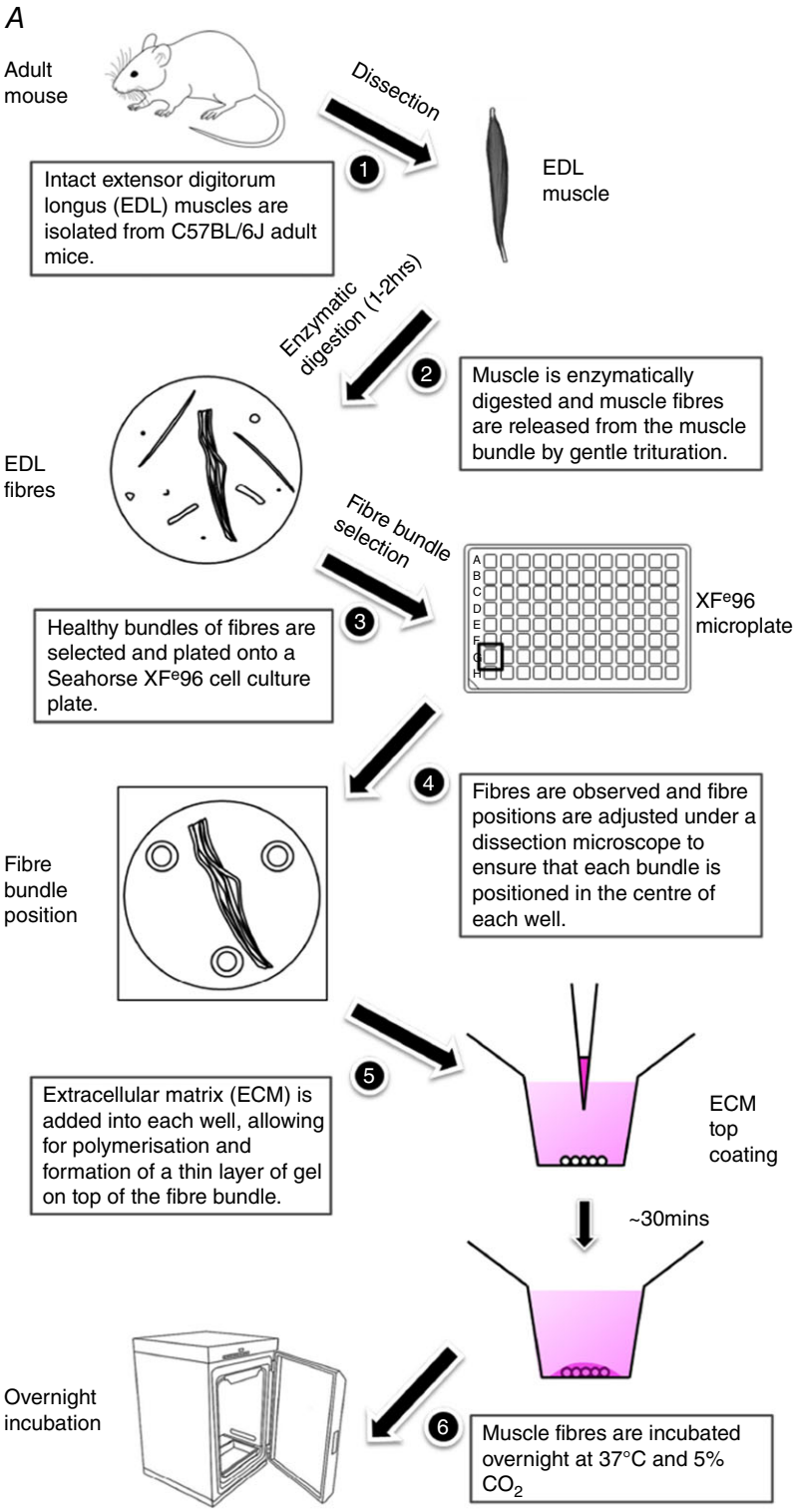

Figure 1. Procedural workflow
A, mouse extensor digitorum longus (EDL) muscle fibre isolation and plate seeding (day 1). *B*, fibre viability normalisation and the Seahorse XF^{e}96 assay run (day 2). [Colour figure can be viewed at wileyonlinelibrary.com]

(n = 4). Mice were housed in a 12 h light, 12 h dark cycle (on at 0600 h and off at 1800 h) and had free access to food (19.6% protein, 4.6% fat; Specialty Feeds, Glen Forrest, Western Australia, Australia) and water unless otherwise specified. Room temperature was maintained at 22 ± 2°C and mice were provided with standard woodchip bedding, tissue paper, enviro-dri and cardboard rolls. Prior to the muscle dissection, mice were anaesthetised with an intraperitoneal injection of sodium pentobarbitone (32.5 mg kg^{-1}, 1PO643-1; Virbac Animal Health, Milperra, New South Wales, Australia). Following complete loss of the pedal withdrawal reflex, mice were killed by cervical dislocation.

Metabolically impaired mouse model

Starting at 8 weeks of age, C57BL/6J male mice were randomly assigned and maintained on either standard mouse chow (Chow: n = 4; 19.6% protein, 4.6% fat; Specialty Feeds) or a commercial high fat diet (HFD: n = 5; 22.6% protein, 23.5% fat; SF04-001, Specialty Feeds). Body weight was assessed at weekly intervals. Following 25 weeks of dietary intervention, glucose tolerance tests were performed as described previously (Huang *et al.* 2012). Mice were allowed 2 days to recover prior to killing (for collection of muscle) and for assessment of body composition, epigonadal and inguinal fat mass, and circulating levels of insulin. At collection, mice were anaesthetised with an intraperitoneal injection of sodium pentobarbitone (32.5 mg kg^{-1}), and whole body fat mass (FM) and fat-free mass (FFM) were immediately determined using nuclear magnetic resonance (Bruker LF50; Bruker, Billerica, MA, USA). Following complete loss of the pedal withdrawal reflex, a single terminal blood sample was collected and assessed for circulating levels of insulin (Steyn *et al.* 2013). Mice were decapitated and muscle tissue was collected for assessment. At the same time, inguinal and epigonadal fat pad weights were isolated and extracted, and immediately weighed (Steyn *et al.* 2013; Stout *et al.* 2016).

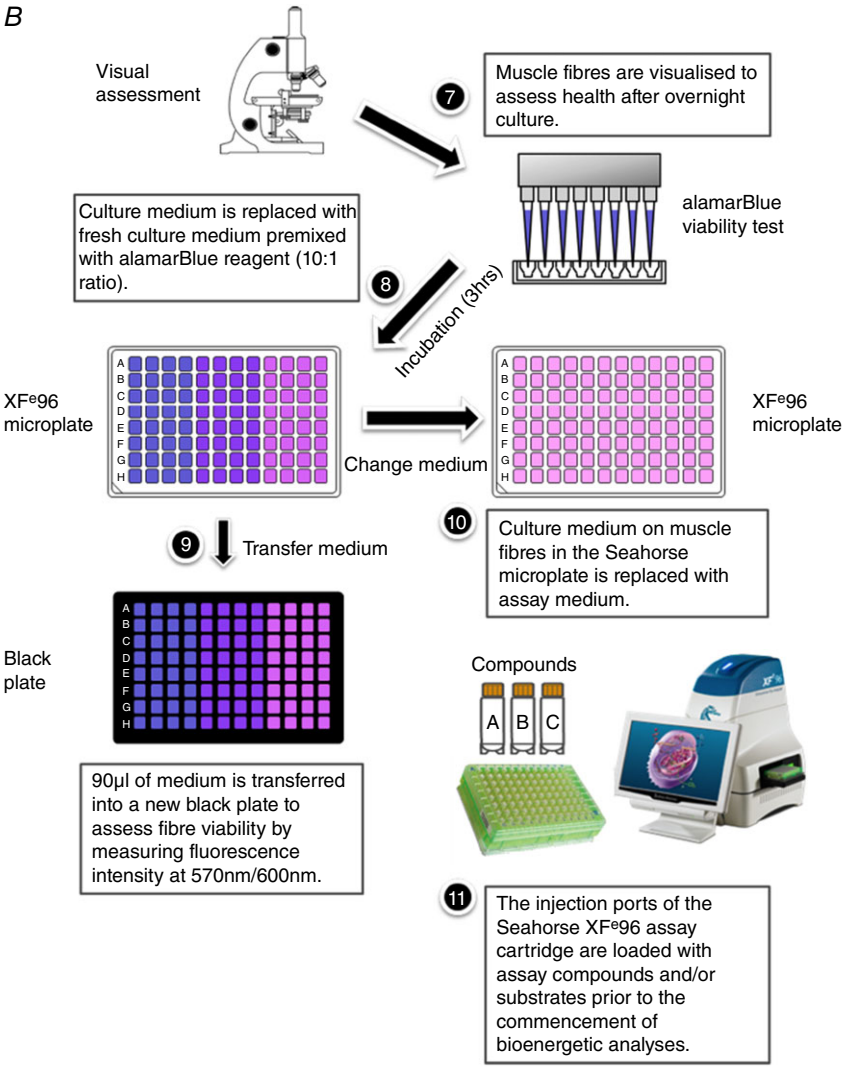

Figure 1. Continued

Isolation of intact EDL fibres

Muscle tissues were processed immediately following collection. Hindlimbs were severed above the knee joint and fully submerged in room temperature Tyrode solution consisting of (mM): 5.4 KCl, 1 $MgCl_2$, 140 NaCl, 0.33 NaH_2PO_4, 2 $CaCl_2$, 10 D-glucose and 10 Hepes (pH 7.4). EDL muscles were dissected out from the hindlimbs (Fig. 1*A*, 1). Both the proximal and distal tendons were kept during dissection to ensure that the EDL muscle was obtained intact and without damage. Fibrous tissue, fat and blood vessels were removed from the EDL muscle using fine forceps under magnification. Each muscle was placed in a 24-well plate well containing 1 ml of low glucose Dulbecco's modified Eagle's medium (DMEM; 12320-032, Thermo Fisher Scientific, Waltham, MA, USA) supplemented with 2.5 mg ml^{-1} collagenase type II (CLS2, 250 u mg^{-1}, Worthington Biochemical Corp., Lakewood, NJ, USA) and 1% antibiotic–antimycotic (15240-062, Thermo Fisher Scientific). Approximately 1 h to 1 h 20 min following harvest and incubation at 37°C and 5% CO_2, each muscle was washed and transferred into a well in a new six-well plate with fresh culture medium containing

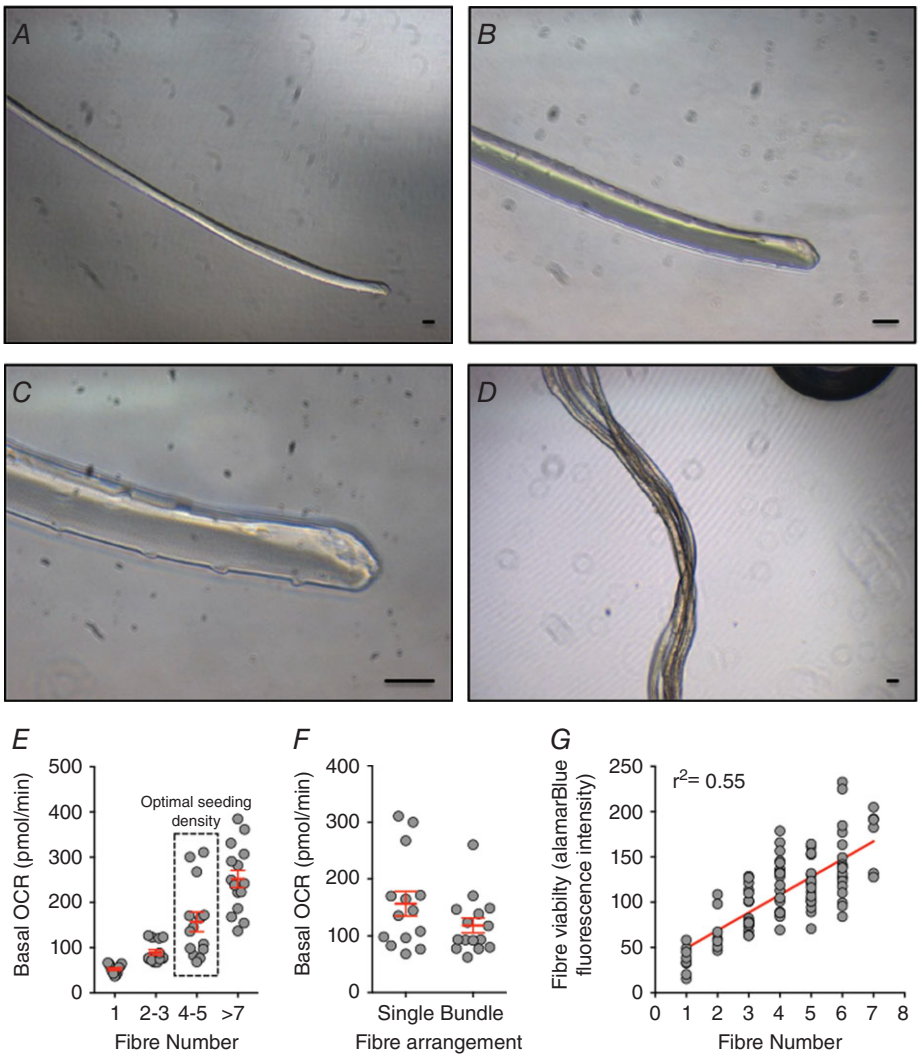

Figure 2. Validation and optimisation of the muscle fibre seeding procedure
A–D, representative examples of intact single extensor digitorum longus (EDL) muscle fibre (*A–C*) and small EDL fibre bundles (*D*). Scale bars: 50 μm. Seeding densities were optimised using single EDL fibres and EDL fibre bundles. *E*, basal oxygen consumption rate (OCR) readings from single fibres ($n = 11$), 2–3 single fibres ($n = 14$), 4–5 single fibres ($n = 14$) and 7–10 single fibres ($n = 15$). Wells containing 4–5 single fibres yielded an optimal basal OCR reading between 100 and 200 pmol min^{-1}. *F*, basal OCR readings from 4–5 single EDL fibres ($n = 14$) and small EDL fibre bundles containing 4–5 myofibres ($n = 15$). The use of small EDL fibre bundles resulted in optimal basal OCR with less variance than multiple single fibres. *G*, the fluorescence intensity of the alamarBlue cell viability assay was linearly correlated with EDL fibre numbers (total $n = 94$). [Colour figure can be viewed at wileyonlinelibrary.com]

low glucose DMEM, 10% fetal bovine serum (FBS; SFBS-F, Bovogen Biologicals, Keilor East, Victoria, Australia) and 1% antibiotic–antimycotic. EDL muscles were gently triturated through a large-bore fire-polished glass pipette (Fig. 1*A*, 2). When the edge of the muscles started to loosen, they were gently flushed with warm medium until fibres were naturally released (Calderon *et al.* 2010). Intact single fibres or small bundles of fibres (containing approximately 5 myofibres) were washed in medium, and transferred using a small-bore fire-polished glass pipette into a new well full of fresh warm culture medium. The transfer of muscle fibres was completed within 10 min. The entire isolation and plating procedure was completed within 1.5 h from harvest (Fig. 2*A*–*C*). The success of the isolation procedure was confirmed qualitatively by field stimulation to induce myofibre contractions following muscle isolation and overnight culture. To avoid rapid fluctuations in the pH and temperature of the medium, DMEM supplemented with 25 mM Hepes was used as the base medium for muscle trituration and fibre culturing, and plates were returned to the incubator at 10 min intervals to allow for medium re-equilibration for 10 min.

Loading EDL fibres onto the XF^{e}96 cell culture microplate

Single EDL fibres, multiple single fibres, or fibre bundles were transferred into each well of a Seahorse XF^{e}96 cell culture microplate (Seahorse Bioscience, Agilent Technologies, Santa Clara, CA, USA) with 150 μl of culture medium (low glucose DMEM supplied with 10% FBS) (Fig. 1*A*, 3). In accordance with Seahorse Extracellular Flux Analyser protocols, the four corner wells (A1, A12, H1 and H12) that were not loaded with fibres stood as temperature control, background wells. Muscle fibres were positioned into the centre of each well by gently pipetting the culture medium without touching the fibres. Fibre positioning was visually verified under a dissecting microscope (Figs. 1*A* (4) and 2*D*), and 2 μl of extracellular matrix (ECM; E1270, Sigma-Aldrich, St Louis, MO, USA) was then added into each well (Fig. 1*A*, 5). The EDL fibres were cultured overnight at 37°C with 5% CO_2 in a standard cell culture incubator (oxygen tension was maintained close to 20%, equivalent to ∼150 mmHg; Figs 1*A*, 6).

Measuring muscle fibre viability and respiration

Fibre samples were visually verified under an inverted microscope after overnight culture (Fig. 1*B*, 7). Before commencing the Seahorse XF assay, the culture medium was replaced with fresh warm culture medium supplemented with 10% alamarBlue cell viability reagent (DAL1025, Thermo Fisher Scientific) (Fig. 1*B*, 8). The alamarBlue reagent is a proven, non-toxic, quantitative cell viability test. The active ingredient is cell permeant, non-fluorescent resazurin, which is continuously reduced in living cells to the fluorescent compound resorufin. Thus, the fluorescence level of the alamarBlue assay medium is proportional to the number of living (viable) muscle cells. The plate was incubated for 3 h to allow fibres to convert resazurin (blue colour, non-fluorescent) to resorufin (red colour, highly fluorescent). Ninety microlitres of medium was then transferred from each well into a black 96-well plate (3991, Corning Inc., Corning, NY, USA) (Fig. 1*B*, 9). The fluorescence signal was read at E_x 570 nm/E_m 600 nm using a SpectraMax M4 microplate reader (Molecular Devices, Sunnyvale, CA, USA). Muscle fibre viability was used for normalisation during data analysis. Subsequent real-time assessment of EDL muscle fibre respiration was performed on the XF^{e}96 Extracellular Flux Analyser.

Seahorse XF mitochondrial stress assay

The mitochondrial stress assay was conducted in assay medium containing: XF base medium (103193-100, Seahorse Bioscience), 4.5 mM D-glucose (G8270, Sigma-Aldrich), 2 mM sodium pyruvate (P2256, Sigma-Aldrich) and 2 mM L-glutamine (25030-081, Thermo Fisher Scientific). Medium was freshly prepared and adjusted to pH 7.4 at 37°C prior to use. Fibres were gently washed twice with 150 μl of pre-warmed assay medium, and all but 20 μl of medium was removed from all the wells after the last wash. Pre-warmed assay medium (180 μl) was then added to each well to reach a final volume of 200 μl (Fig. 1*B*, 10). The assay plate was placed into the Seahorse XF prep station (37°C incubator, without CO_2; Seahorse Bioscience) for 1.5 h to de-gas. Meanwhile, oligomycin A, carbonyl cyanide-*p*-trifluoromethoxyphenylhydrazone (FCCP) and antimycin–rotenone reagents (Seahorse Bioscience) were prepared with assay medium and loaded into ports A, B and C of the XF^{e}96 sensor cartridge (25 μl per port), respectively, to allow sequential injection of compounds to induce mitochondrial stress in EDL fibres. The final working concentrations of oligomycin A, FCCP and antimycin–rotenone were 1.0, 0.4 and 1.0 μM, respectively. Following de-gassing, the assay plate and the pre-loaded cartridge were placed into the XF^{e}96 analyser (Fig. 1*B*, 11). Oxygen consumption rate (OCR) and extracellular acidification rate (ECAR) were continuously recorded for 12 cycles, with each cycle consisting of 3 min of mix, 30 s of wait and 3 min of measurement (M). The first three cycles (M1–3) measured basal respiration. Subsequent to this, three cycles were run following each injection of oligomycin A (M4–6), FCCP (M7–9) and antimycin–rotenone (M10–12). The mitochondrial parameters measured through this assay included ATP turnover (the decrease in OCR upon the injection of the ATP synthase inhibitor oligomycin), proton-leak (the remaining mitochondrial OCR upon

injection of oligomycin), and spare respiratory capacity in EDL fibre bundles (the difference between basal OCR and FCCP-induced maximal OCR).

Pyruvate- and palmitate-induced maximal respiration

To test substrate use in EDL fibre bundles, the assay medium was modified to contain (mM) 120 NaCl, 3.5 KCl, 1.3 $CaCl_2$, 0.4 KH_2PO_4, 1 $MgCl_2$, 2.5 D-glucose and 0.5 L-carnitine (C0158, Sigma-Aldrich) (Schuh *et al.* 2012, 2014). The assay medium was freshly prepared on the day of the assay and kept at 37°C. The pH of the assay medium was adjusted to 7.4 before the medium exchange to minimise the pH change. Fibres were gently washed twice with 150 μl of pre-warmed assay medium, with all but 20 μl of medium being removed from all the wells after the last wash. Pre-warmed assay medium (180 μl) was then added to each well to reach a final volume of 200 μl (Fig. 1*B*, 10). Fibres were placed into the XF prep station and de-gassed for 1.5 h. Either sodium pyruvate (P2256, Sigma-Aldrich) or palmitate–BSA (102720-100, Seahorse Bioscience) was loaded into port A with FCCP (25 μl total volume per port), and antimycin–rotenone was loaded into port B (25 μl per port) of the sensor cartridge to allow sequential injections of compounds to assess mitochondrial respiratory capacity in the presence of different energy substrates (Fig. 1*B*, 11). The assay was run as follows: nine cycles of 3 min of mix, 30 s of wait and 3 min of measurement. After three cycles of basal measurement (M1–3), either sodium pyruvate (final working concentration, 10 mM) or palmitate–BSA (final working concentration, 100 μM) was injected with FCCP (final working concentration, 0.4 μM), after which, three cycles (M4–6) were recorded to determine induced maximal mitochondrial respiration in EDL fibres. The last three cycles (M7–9) were recorded following the injection of antimycin–rotenone (final working concentration, 1.0 μM).

Statistical analysis

Statistical differences were assessed using Prism 6.0h (GraphPad Software, La Jolla, CA, USA). For body weight change and glucose response, differences between Chow and HFD mice were assessed by two-way ANOVA and Bonferroni multiple comparisons tests. All other measures from mice were compared using Student's unpaired *t* test. Raw data were retrieved from the XF^{e}96 analyser Wave software (version 2.2). Repeated measures ANOVA was used to compare basal OCRs at the first three measurements and after the injection of assay medium control. Student's paired *t* test was used to compare chemical induced OCR and ECAR changes with basal levels. An independent *t* test was used to compare the area under the curve (AUC) of OCR and ECAR between pyruvate and palmitate treated groups. All metabolic flux experiments were performed three times and data are presented as the mean ± SEM. Values of $P < 0.05$ were considered as statistically significant.

Results

Optimal muscle fibre culture conditions

We optimised medium pH and culturing temperature to improve the yield and viability of muscle fibres. The pH of the culture medium during muscle fibre isolation was maintained at approximately 7.4 with Hepes supplement (Westerblad *et al.* 1997). Without Hepes, the pH of the DMEM rapidly turned alkaline (pH > 7.6) when left outside of the 5% CO_2 incubator, and EDL fibres started to degrade. Isolated EDL fibres exhibited tolerance towards lower temperatures; intact EDL single fibres and fibre bundles cultured in a 5% CO_2 incubator at either 30°C or 37°C remained viable. As we observed no difference in fibre survival between the two temperatures after overnight culture, 37°C was selected as the experimental temperature (Talan, 1984). To test whether muscle fibre viability could be improved by the presence of serum supplements, EDL fibres were isolated and cultured in either serum-free DMEM or DMEM supplemented with 10% FBS. Releasing and culturing fibres in a serum-free environment led to fibre degradation, while the presence of 10% FBS led to improved preservation of fibre viability.

Optimal muscle fibre seeding and assay normalisation

Basal OCRs of single EDL fibres, 2–3 single fibres, 4–5 single fibres and 7–10 single fibres were 52.64 ± 3.23, 89.19 ± 6.16, 157.03 ± 21.83 and 251.78 ± 19.20 pmol min^{-1} respectively (Fig. 2*E*). While we observed an increase in the variance in OCR with increasing fibre number (> 3 fibres; Fig. 2*E*) due to difficulties with maintaining consistency in sample positioning among wells, seeding of 4–5 single EDL fibres per well yielded an optimal basal OCR between 100 and 200 pmol min^{-1}. This optimal basal OCR provides a better signal to noise ratio and dynamic response towards mitochondrial stimulus (Rogers *et al.* 2011). The placement of multiple single fibres into each well greatly increased the duration of sample preparation and thus time outside of the incubator, compromising muscle fibre viability. To minimise working time, small fibre bundles containing 4–5 myofibres were selected to test basal respiration. Compared with 4–5 multiple single fibres, these myofibre bundles yielded an optimal basal OCR of 120 ± 13.86 pmol min^{-1} with less variability (Fig. 2*F*). Thus, EDL fibre bundles were used for subsequent experiments.

Due to the small number of fibres in each well, we were unable to normalise Seahorse XF assay results to protein content determined using a conventional BCA assay (Pierce BCA Protein Assay Kit, Thermo Fisher Scientific). Therefore, we developed an alternative approach, wherein assay results were normalised to alamarBlue fluorescence intensity. The fluorescence intensity of the alamarBlue assay is positively correlated with the number of EDL fibres (Fig. 2*G*), and thus provides a quantitative estimate of muscle tissue content per well.

Inducing maximal mitochondrial respiration in EDL fibre bundles

To verify whether cellular respiration in EDL fibre bundles could be recorded steadily over the whole assay, 25 μl of assay medium was injected through ports A, B and C onto fibres after measurements 3, 6 and 9 (Fig. 3*A*). The basal OCR of the first measurement cycle was 122.36 $\pm$ 13.35 pmol min^{-1}. Basal OCR did not change throughout the assay period.

To determine key parameters of mitochondrial respiration in EDL fibre bundles, OCRs and ECARs were measured under the basal state and during FCCP-induced maximal respiration after sequential exposure to the ATP synthase inhibitor oligomycin A, the uncoupler FCCP and the ETC inhibitors antimycin and rotenone. Oligomycin A was injected onto EDL fibre bundles at doses ranging from 0.25 to 2.0 μM to determine the optimal working concentration that would effectively inhibit ATP production without causing cellular respiration collapse (Fig. 3*B* and *C*); 0.4 μM FCCP and 1.0 μM antimycin–rotenone were then injected respectively. No change in OCR was observed after 0.25 or 0.5 μM oligomycin A injection. We found that 1.0 μM oligomycin A was optimal to inhibit ATP production-related respiration in EDL fibre bundles, while allowing for detection of maximal respiration capacity. However, the success rate of oligomycin A inhibition of OCR in EDL fibre bundles was relatively low at approximately 52% in the 1.0 μM oligomycin A group.

The mitochondrial stress assay data for EDL fibre bundles are shown in Fig. 4*A*–*G*. Basal OCR readings were consistent for the first three measurements, resulting in a basal OCR of 120.29 $\pm$ 16.15 pmol min^{-1} at M3. Since the OCR and ECAR readings were most stable at M3, we set this measurement point as the baseline of Seahorse XF assays for data analyses. Injection of 1.0 μM oligomycin A resulted in a drop in the OCR to 89.84 $\pm$ 13.87 pmol min^{-1} at M6. Following application of 0.4 μM FCCP, maximal respiration was induced and the OCR reading increased to 246.06 $\pm$ 19.46 pmol min^{-1} at M7. Antimycin–rotenone at 1.0 μM blocked mitochondrial respiration and reduced OCR to 37.88 $\pm$ 8.48 pmol min^{-1} at M12 (Fig. 4*A* and *B*). Mitochondrial parameters, such as ATP turnover, proton leak, and spare respiratory capacity in EDL fibre bundles, were determined by calculating OCR percentage changes after the assay (Fig. 4*C*). ATP synthesis-related respiration, proton leak and non-mitochondrial respiration contributed to 26.06 $\pm$ 3.91%, 39.03 $\pm$ 8.32% and 34.91 $\pm$ 6.77% of the basal OCR. The ATP turnover and proton leak accounted

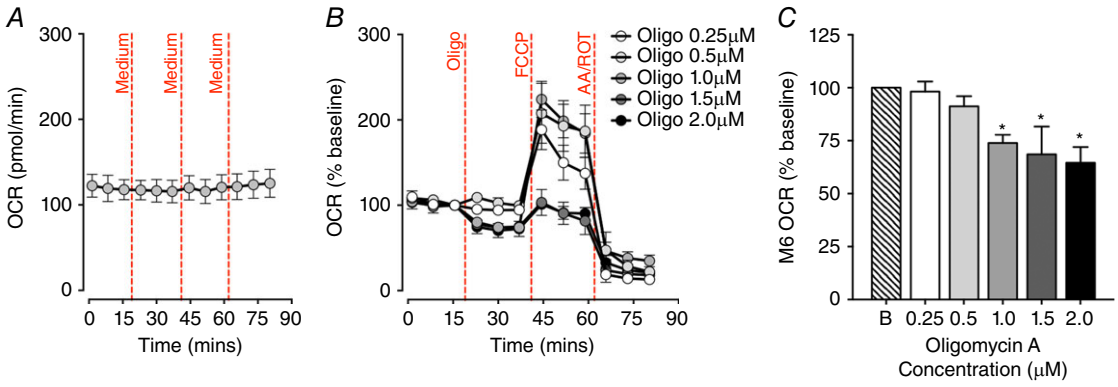

Figure 3. Optimisation of the mitochondrial stress test using extensor digitorum longus (EDL) muscle fibre bundles
A, basal oxygen consumption rate (OCR) readings of EDL fibre bundles remained stable throughout the 80 min of measurement in response to three injections of assay medium (n = 5). *B*, optimal inhibition of ATP-coupled OCR in EDL fibre bundles by oligomycin A (Oligo, 0.25-2.0 μM), followed by injections of carbonyl cyanide-*p*-trifluoromethoxyphenylhydrazone (FCCP, 0.4 μM) and antimycin–rotenone (AA/ROT, 1.0 μM). *C*, baseline normalised OCR levels at the sixth measurement cycle (M6), after different working concentrations of oligomycin A were injected to inhibit ATP synthesis in EDL fibre bundles. Oligomycin A at 0.25 or 0.5 μM did not decrease the OCR when compared with the basal OCR, while oligomycin A at a working concentration of 1.0 μM or above induced a significant inhibition of OCR in EDL fibre bundles (oligomycin A groups: 0.25 μM, n = 9; 0.5 μM, n = 12; 1.0 μM, n = 10; 1.5 μM, n = 5; 2.0 μM, n = 6; $^*P < 0.05$, compared with baseline (B)). [Colour figure can be viewed at wileyonlinelibrary.com]

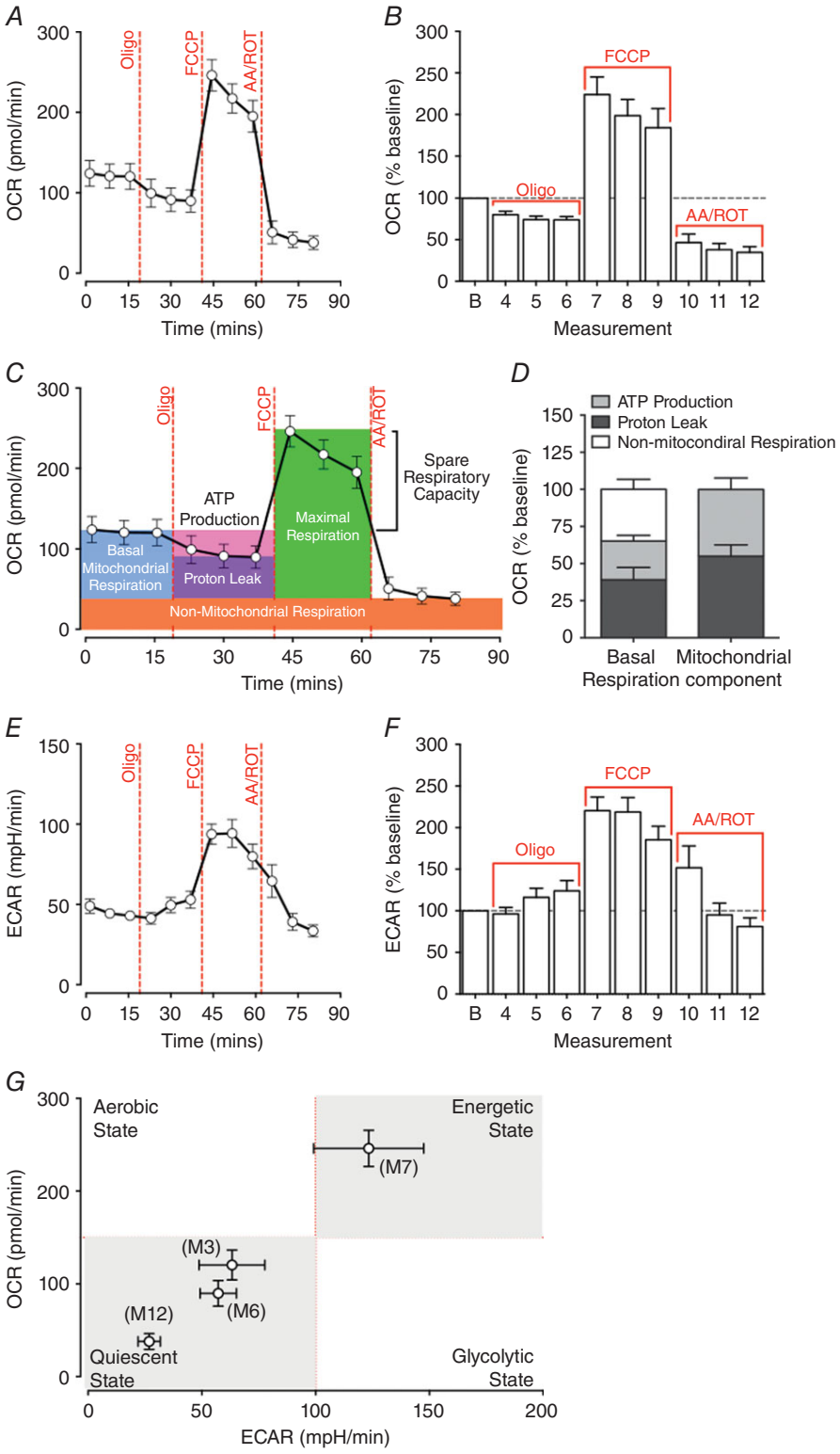

Figure 4. Biogenetic profiles of extensor digitorum longus (EDL) muscle fibre bundles under the basal condition and during FCCP-induced maximal respiration
A and *B*, absolute values (*A*) and baseline normalised oxygen consumption rate (OCR; *B*) were determined in EDL fibre bundles at baseline and after FCCP-induced maximal respiration. OCR levels were inhibited by oligomycin A to 73.94 ± 3.91% of the baseline at the sixth measurement cycle (M6) and surged to 224.05 ± 21.03% of the baseline at M7 following the injection of FCCP. *C*, key parameters of mitochondrial respiration in EDL fibre

for 45.00 ± 7.67% and 55.00 ± 7.67% of mitochondrial respiration respectively (Fig. 4*D*).

The basal ECAR of EDL fibre bundles was 43.03 ± 2.23 milli-pH units (mpH) min^{-1} at M3. Although oligomycin A slightly increased the ECAR to 124.01 ± 12.40% at M6 relative to the baseline, there was no significant change in ECAR between baseline and after the injection of oligomycin A ($P = 0.170$, repeated measures ANOVA, M1–6). FCCP significantly increased the ECAR to 93.76 ± 7.08 mpH min^{-1} at M7 ($P = 0.001$ compared with M3). The ECAR remained high at M8 and M9. Antimycin and rotenone reduced the ECAR to 34.41 ± 4.03 mpH min^{-1} at M12 (Fig. 4*E* and *F*).

The energetic phenotype of EDL fibre bundles at rest and following forced maximal respiration was mapped by plotting paired OCR and ECAR for each measurement point. In Fig. 4*G*, the four quadrants represent four metabolic states: quiescent state (low OCR, low ECAR), aerobic state (high OCR, low ECAR), energetic state (high OCR, high ECAR) and glycolytic state (low OCR, high ECAR). EDL fibres exhibited the low OCR and ECAR quiescent profile at the basal state (M3), after exposure to oligomycin (M6) and after exposure to antimycin–rotenone (M12). However, after the injection of FCCP, both OCR and ECAR greatly increased at M7, indicating that mitochondrial oxidative phosphorylation and glycolysis pathways were actively recruited to meet maximal energy needs.

Pyruvate- and palmitate-induced respiration

To demonstrate that this method can be used to assess substrate utilisation, we determined pyruvate- and palmitate-induced respiration in isolated EDL fibre bundles (Fig. 5*A* and *B*). FCCP was added in combination with the substrate to enable the maximal use of pyruvate or fatty acid. By dissipating the proton gradient across the inner mitochondrial membrane, FCCP abolished the rate-limiting effect of substrate transportation and allowed for the induction of maximal mitochondrial respiration (Hus-Citharel & Morel, 1986; To *et al.* 2010).

There was no significant difference in basal OCR between the pyruvate-treated group and palmitate-treated group (Fig. 5*C*). Injection of 10 mM pyruvate and 0.4 μM FCCP increased OCR to 228.47 ± 22.73 pmol min^{-1} at M4 ($P < 0.001$ compared to basal OCR at M3; Fig. 5*A*). However, the OCR quickly returned to basal levels at M5 (144.30 ± 22.64 pmol min^{-1}) and M6 (88.97 ± 24.08 pmol min^{-1}) (Fig. 5*A*). Application of 100 μM palmitate–BSA and 0.4 μM FCCP induced a sustained level of high OCR. OCR was maintained at 277.98 ± 23.38, 231.32 ± 14.60 and 187.76 ± 23.89 pmol min^{-1} at M4, M5 and M6 respectively ($P < 0.001$ compared to basal OCR at M3; Fig. 5*A*). Following exposure to 1.0 μM antimycin and rotenone, the OCR at M9 dropped to 23.41 ± 2.32 pmol min^{-1} in the pyruvate group and 44.71 ± 9.51 pmol min^{-1} in the palmitate–BSA group (both $P < 0.001$ compared to M3; Fig. 5*A*). The AUC of OCR in the pyruvate group (5803.71 ± 605.60 pmol) was significantly lower than that of the palmitate group (8316.20 ± 683.64 pmol) ($P = 0.013$; Fig. 5*E*).

There was no significant difference in the basal ECAR between the pyruvate- or palmitate-treated groups (Fig. 5*D*). In the pyruvate group, the ECAR increased to 98.70 ± 9.03 mpH min^{-1} at M4 ($P < 0.001$ compared to basal ECAR at M3; Fig. 5*B*) and declined to baseline at M6 (Fig. 5*B*). The ECAR quickly dropped after exposure to antimycin–rotenone, declining to 33.51 ± 3.25, 33.80 ± 2.81 and 30.20 ± 3.26 mpH min^{-1} at M7, M8 and M9, respectively (all $P < 0.05$ compared to basal ECAR at M3; Fig. 5*B*). Treatment of fibres with palmitate led to an increase in ECAR to 99.77 ± 10.34 mpH min^{-1} at M4 and 96.32 ± 10.54 mpH min^{-1} at M5 (both $P < 0.01$ compared to M3; Fig. 5*B*). After the mitochondrial ETC was blocked by antimycin–rotenone, the ECAR was sustained at the basal level at measurement M9 (Fig. 5*B*). The total acidification (AUC of the ECAR) was significantly higher in the palmitate group compared to the pyruvate group ($P < 0.05$; Fig. 5*F*).

Reduced resting respiration and enhanced oxidation activity in response to FCCP-induced maximal respiration in HFD EDL fibre bundles

To demonstrate the application of this method for measuring muscle bioenergetics in a metabolic disease

bundles determined by the mitochondrial stress assay. Oligomycin A inhibits ATP production-related mitochondrial respiration, but does not prevent oxygen consumption through proton leak. Mitochondrial electron transport chain (ETC) complex I and III inhibitors antimycin and rotenone completely shut down mitochondrial oxygen consumption, leaving non-mitochondrial-related respiration. *D*, percentage proportions of ATP turnover, proton leak and non-mitochondrial respiration contributed to total basal respiration and mitochondrial respiration in EDL fibre bundles. *E* and *F*, absolute values (*E*) and baseline normalised extracellular acidification rate (ECAR; *F*) from EDL fibre bundles. ECAR peaked at M7 following the injection of FCCP, accounting for 220.43 ± 16.36% of baseline respiration. *G*, matched OCRs and ECARs of EDL fibre bundles at the 3rd, 6th, 7th and 12th measurement, representing the energy phenotype at the basal state (M3) and after the exposure of oligomycin A (M6), FCCP (M7) and antimycin–rotenone (M12). The EDL fibre bundles switched to a high oxidative phosphorylation and high glycolysis phenotype under FCCP-induced maximal respiration ($n = 10$). [Colour figure can be viewed at wileyonlinelibrary.com]

model, we compared the changes in basal respiration and fuel oxidation capacity of EDL muscle fibre bundles obtained from chronic high-fat fed mice and chow-fed (control) mice. Maintenance of mice on a high-fat diet (HFD) promoted progressive weight gain (Fig. 6*A*), resulting in an increase in total body weight (Fig. 6*B*) and an overall increase in adiposity (Fig. 6*C*) and epigonadal and inguinal fat mass (Fig. 6*D*). Dietary-induced weight gain resulted in the impairment of blood glucose clearance (as assessed by intraperitoneal glucose tolerance testing; Fig. 6*E* and *F*), an overall rise in fasting blood glucose levels (Fig. 6*G*), and a rise in circulating levels of insulin during the postprandial state (Fig. 6*G*). Collectively, these observations are reminiscent of dietary-induced obesity and impaired glucose metabolism found in metabolic syndrome and insulin resistance. We next assessed the metabolic capacity and substrate use of isolated EDL muscle fibres of HFD and chow-fed mice. The normalised baseline OCR in EDL muscle fibre bundles from HFD mice was lower (0.97 ± 0.15 pmol min^{-1} (fluorescence intensity)$^{-1}$) when compared to EDL fibre bundles from chow-fed mice (0.53 ± 0.02 pmol min^{-1} (fluorescence intensity)$^{-1}$; $P = 0.01$, independent *t* test; Fig. 6*H* and *I*). The normalised basal ECAR in EDL fibre bundles from HFD and chow-fed mice did not differ (Fig. 6*K* and *L*). In contrast to the quiescent metabolic phenotype shown at rest, EDL fibre bundles from HFD mice demonstrated an enhanced capacity to oxidise pyruvate or palmitate following FCCP-induced uncoupling (Fig. 6*J*). Compared with the fibre bundles from chow-fed mice, fibre bundles from HFD mice exhibited higher baseline normalised OCR peaks at M4 when using either pyruvate ($P < 0.001$, independent *t* test) or palmitate ($P = 0.049$, independent *t* test) as the energy source (Fig. 6*H*). There was an instant ECAR peak (Fig. 4*K*) at M4 in the pyruvate-treated muscle fibre bundles from chow-fed mice without a corresponding change in OCR (Fig. 6*H*). The AUCs of baseline normalised OCR ($P < 0.001$, independent *t* test, Fig. 6*J*) and ECAR ($P = 0.002$, independent *t* test, Fig. 6*M*) were significantly higher in EDL fibre bundles from mice maintained on the HFD when compared to muscle fibre bundles from chow-fed mice when pyruvate was supplied as the main energy source (Fig. 6*M*).

Discussion

Analysis of cellular bioenergetics in skeletal muscle presents an opportunity to better understand muscle metabolism in health and disease. Here we present a method that allows for the real-time measurement of cellular respiration in intact long skeletal muscle fibre bundles in a 96-well microplate format. By conducting bioenergetic analysis in live EDL fibre bundles within 24 h of isolation, our study provides an approach to assess metabolic flux in fully differentiated adult muscle fibres that maintain their metabolic phenotypes (Schuh *et al.* 2012; Archacka *et al.* 2014).

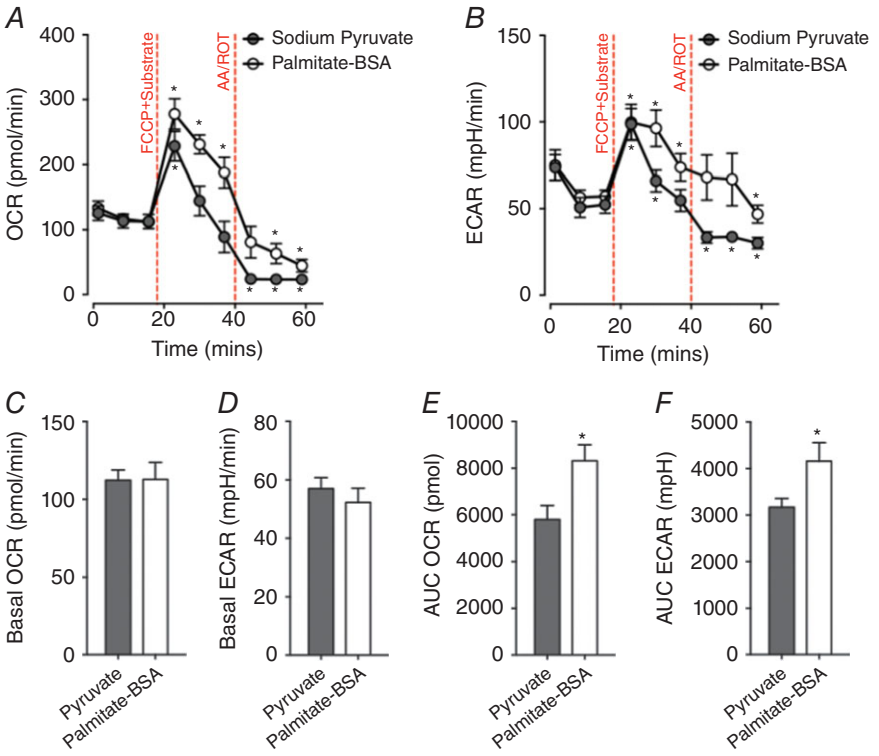

Figure 5. Differential capacity of extensor digitorum longus (EDL) muscle fibre bundles to utilise pyruvate or palmitate in response to FCCP-induced maximal respiration
A and *B*, absolute values of (*A*) oxygen consumption rate (OCR) and extracellular acidification rate (ECAR; *B*) at each measurement cycle. EDL fibre bundles utilising palmitate ($n = 10$) maintained high OCR and ECAR levels for longer than fibres utilising pyruvate ($n = 10$; $^*P < 0.05$, compared with basal measurements). *C* and *D*, no difference of basal OCR level or ECAR level was observed between pyruvate and palmitate–BSA treated groups. *E* and *F*, EDL fibre bundles exposed to palmitate had higher total OCR and total ECAR (as defined by the area under the curve; AUC) when compared to fibres exposed to pyruvate ($^*P < 0.05$). [Colour figure can be viewed at wileyonlinelibrary.com]

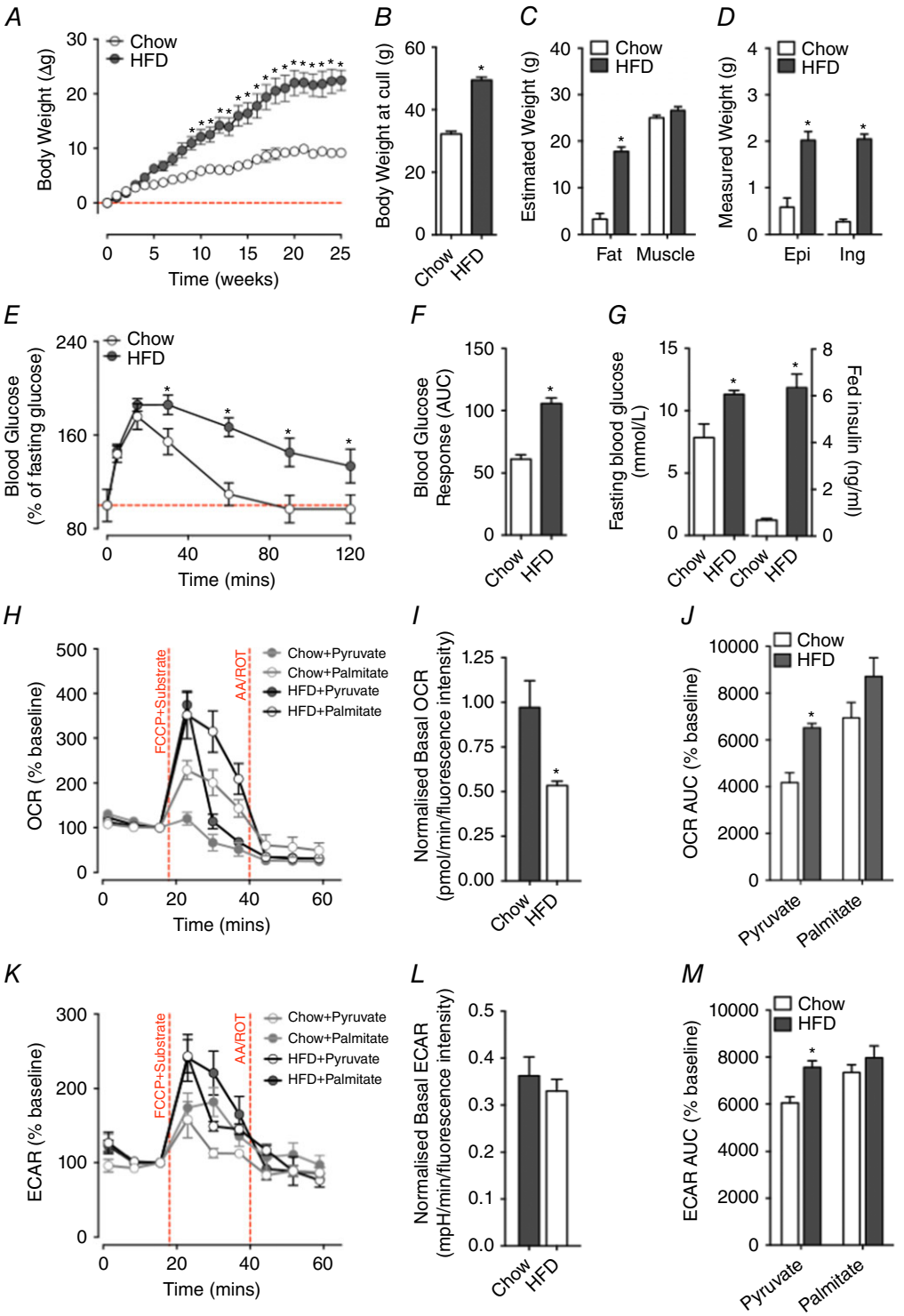

Figure 6. Systemic impairments in glucose tolerance enhance mitochondrial oxidation capacity in extensor digitorum longus (EDL) muscle fibre bundles while lowering the basal respiration
A–D, maintenance of mice on a high-fat diet (HFD) promotes weight gain (*A* and *B*) due to increased fat mass (total, epigonadal (Epi) and inguinal (Ing)) (*C* and *D*). *E–G*, this occurs alongside a worsening of blood glucose clearance (*E* and *F*), and an elevation in fasting levels of blood glucose and a rise in plasma insulin levels in the fed state (*G*). Collectively, these measures are indicative of metabolic syndrome associated with insulin resistance. *I*, basal OCR (normalised to alamarBlue) of EDL muscle fibre bundles is significantly reduced in HFD mice when compared to mice maintained on a standard chow diet. *L*, by contrast, basal ECAR (normalised to alamarBlue)

Historically, the assessment of mitochondrial function in isolated skeletal muscle fibres has been limited to short fibres isolated from the flexor digitorum brevis (FDB) or interossei muscle (Bruton *et al.* 2003; Rossi *et al.* 2011). Given that mitochondrial content and bioenergetic signatures differ among muscle fibre types (Isaeva *et al.* 2005; Tricarico *et al.* 2006; Mackrell & Cartee, 2012), the adoption of intact long skeletal muscle fibres for bioenergetic assessment allows one to obtain a greater understanding of muscle metabolism. Thus, we established a method that would generate a large yield of viable and intact EDL fibre bundles for metabolic assessment. In accordance with previous studies (Brown & Schneider, 2002; Calderon *et al.* 2010; Archacka *et al.* 2014), we confirm that 37°C was the optimal temperature for mouse EDL muscle digestion and myofibre culturing. In our study, medium pH proved critical for preventing the degradation of myofibres. Moreover, we found that supplementation of medium with 10% FBS resulted in improved morphology and quality of EDL fibres. This is not surprising since an absence of FBS in culture medium results in the supercontraction of mouse muscle fibres (Selvin *et al.* 2015). By implementing an on-top ECM coating method, we were able to secure the position of fibre bundles, thus greatly minimising the loss of fibres and reducing variability during the Seahorse XF assay. Importantly, EDL fibres remained viable during the whole experimental procedure, and the polymer scaffold structure of the ECM did not prevent the free exchange of nutrients, oxygen and ions between muscle fibres and culture medium. This was confirmed by testing the Seahorse XF mitochondrial stress assay and substrate assay on C2C12 mouse myoblasts and myotubes. No difference in OCR readings was observed between ECM coated and non-ECM coated C2C12 cells (data not presented).

To validate our method, mitochondrial parameters in isolated EDL fibre bundles were measured using a Seahorse XF mitochondrial stress assay. Cell oxygen consumption is recognised as an important index to evaluate mitochondrial function and energy expenditure (Ferrick *et al.* 2008; Brand & Nicholls, 2011). It has been suggested that skeletal muscle has poor mitochondrial coupling; skeletal muscle fibres have high proton leak ratios (35–50%) when compared to most cell types (around 20%) (Brand, 2000, 2005). Indeed, proton leak accounts for 52 $\pm$ 15% of the resting respiration rate in perfused rat hindquarters (Rolfe & Brand, 1996). Moreover, perfused rat hindquarters present with a high 34% proton leak ratio under maximal action tension (Rolfe *et al.* 1999), and proton leak accounts for 29 $\pm$ 2% and 36 $\pm$ 3% of total maximal mitochondrial respiration in the vastus lateralis muscle of young and old adults, respectively (Porter *et al.* 2015). By assessing the bioenergetics of EDL muscle fibre bundles following forced maximal mitochondrial respiration, we demonstrate that approximately half of the mitochondrial OCR was contributed by proton leak. In this regard, the data demonstrate that our method provides an *in situ* approach to measure mitochondrial function in intact skeletal muscle fibre bundles.

To validate the use of this method for the assessment of substrate utilisation, we assessed mitochondrial respiration capacity in EDL fibre bundles when pyruvate or palmitate was provided as energy substrates. In the presence of FCCP, both pyruvate and palmitate could induce peak OCR in EDL fibre bundles. Interestingly, EDL fibres supplied with palmitate maintained a high OCR and ECAR for a longer time, and exhibited higher total levels of oxygen consumption and extracellular acidification when compared to the pyruvate group. This sustained OCR in the presence of palmitate is in line with the notion that fatty acids can metabolically support increased duration of work in skeletal muscle (Weis-Fogh, 1967; Suarez *et al.* 1986).

Dysfunction in glucose and fatty acid metabolism in insulin-resistant skeletal muscle has been intensively studied in HFD-induced obesity and diabetes models (Halseth *et al.* 2000; Suga *et al.* 2014). By measuring muscle pyruvate and palmitate utilisation capacity *in situ*, we revealed a metabolic phenotype transition in EDL fibre bundles isolated from chronic HFD fed mice, from suppressed resting respiration to enhanced mitochondrial oxidation in response to FFCP-induced maximal respiration. Although it has been suggested that high-fat feeding impairs mitochondrial mass and function in skeletal muscle (Simoneau *et al.* 1999; Sparks *et al.* 2005; Morino *et al.* 2006), our current findings are in line with the 'mitochondrial nutrient wasting' concept generated from obesity and diabetes studies, which suggests enhanced, albeit less efficient fuel oxidation in

does not differ between HFD and chow-fed mice. *H* and *K*, to minimise the effects of different basal respiration rate, baseline normalised OCR (*H*) and ECAR (*K*) in EDL muscle fibre bundles of HFD-fed mice and chow-fed mice were determined to assess pyruvate or palmitate utilisation capacity during FCCP-induced maximal respiration. Compared with chow-fed mice, EDL muscle fibre bundles of HFD-fed mice exhibited a higher OCR peak when using pyruvate or palmitate as a principal energy substrate. *J* and *M*, baseline normalised total OCR (*J*) and ECAR (*M*) values in EDL fibre bundles were determined by calculating area under the curve (AUC). When utilising pyruvate as the principal energy source, EDL fibre bundles of HFD-fed mice had higher total OCR and total ECAR values compared to chow-fed controls (pyruvate-treated HFD fibre group: $n = 8$; palmitate-treated HFD fibre group: $n = 8$; pyruvate-treated chow-diet fibre group: $n = 8$; palmitate-treated chow-diet fibre group: $n = 8$; $^*P < 0.05$, compared with chow-fed controls). [Colour figure can be viewed at wileyonlinelibrary.com]

skeletal muscle from high-fat fed mice (Levine *et al.* 1999; Liesa & Shirihai, 2013). Indeed, investigation of isotopic labelled fatty acid β-oxidation intermediates in skeletal muscle from high-fat fed mice has revealed increased mitochondrial content and increased incomplete fatty acid oxidation (Koves *et al.* 2008).

While this method allows for the assessment of metabolic flux in intact muscle fibre bundles, higher throughput of bioenergetic analysis, reduced requirement for repetitive sampling, and the potential to reflect *in situ* fuel utilisation in intact muscle fibres without disturbing cellular structure, some limitations exist. First, total protein normalisation could not yield accurate results due to the high background encountered with the ECM coating. Furthermore, there was increased risk of losing muscle fibres when dissolving the ECM to wash and retrieve fibres for protein quantification. To overcome this, we used alamarBlue as an indicator of fibre viability. The linear correlation between alamarBlue readings and fibre numbers suggest that alamarBlue may be used as a safe and feasible method to normalise muscle fibre numbers in this assay. Use of alamarBlue cannot account for mitochondrial content or quality, and this limitation needs to be addressed if the user suspects differences in these parameters. Secondly, our method does not allow for the confirmation of fibre types within each fibre bundle. Skeletal muscle consists of a mixture of fibre types, which exhibit metabolic phenotypes that range from highly glycolytic to more oxidative (Essen et al. 1975; Gollnick et al. 1985). In different mouse strains, including the C57BL/6J, the soleus contains mainly type I and IIa fibres (Augusto *et al.* 2004), the FDB contains types I, IIa and IIx fibres (Gonzalez *et al.* 2003), and the EDL predominantly contains type IIb fibres and a few IId fibres (Augusto *et al.* 2004; Calderon *et al.* 2009; Banas *et al.* 2011). Given the difference in metabolic patterns between slow oxidative (type I), fast oxidative glycolytic (type IIa) and fast glycolytic (type IIb, IIx) fibres (Isaeva *et al.* 2005; Tricarico *et al.* 2006; Schiaffino & Reggiani, 2011; Mackrell & Cartee, 2012), assessment of mitochondrial respiration, and glucose and fatty acid oxidation profiles using this method will likely be influenced by the type of muscle being assessed. Regardless, the consistent OCR responses that we observed after chemical stimulation indicate that the metabolic profile we measured in EDL muscle was contributed to by fast glycolytic fibres and that this profile is likely to be EDL-specific. Thirdly, the successful response rate of this assay was largely determined by the fibre quality and assay design. Optimisation of muscle fibre isolation and coating conditions was crucial for attaining optimal survival of muscle fibres after overnight culture and during the assay. In this regard, muscle fibres that die or fail to respond throughout the assay are easily identified by a sudden drop in OCR, and should be omitted from subsequent analyses.

In conclusion, we have developed an approach that allows for the real-time assessment of cellular respiration in intact, long skeletal muscle fibre bundles across various muscle subtypes. By using the Seahorse XF^{e}96 platform, we were able to measure mitochondrial parameters from multiple EDL fibre bundle samples during a single assay. This practical approach offers greater experimental flexibility, and meets the increasing needs of higher throughput metabolic analysis of intact muscle fibre bundles. Therefore, the current methodology offers a valuable opportunity to inform the experimenter of potential critical mitochondrial defects. These can then be interrogated using lower-throughput but more selective approaches to define specific defects in mitochondrial function or electron transport chain complexes. It is further anticipated that this method will allow for improved capacity and flexibility to study cellular metabolism across different skeletal muscle fibre lengths and subtypes, and that this methodology could be translated across multiple models, including muscle fibres derived from healthy and patient muscle biopsies.

References

Ahima RS & Park HK (2015). Connecting myokines and metabolism. *Endocrinol Metab (Seoul)* **30**, 235–245.

Archacka K, Pozzobon M, Repele A, Rossi CA, Campanella M & De Coppi P (2014). Culturing muscle fibres in hanging drop: a novel approach to solve an old problem. *Biol Cell* **106**, 72–82.

Augusto V, Padovani CR & Campos GER (2004). Skeletal muscle fiber types in C57BL6J mice. *Braz J Morphol Sci* **21**, 89–94.

Banas K, Clow C, Jasmin BJ & Renaud JM (2011). The K_{ATP} channel Kir6.2 subunit content is higher in glycolytic than oxidative skeletal muscle fibers. *Am J Physiol Regul Integr Comp Physiol* **301**, R916–R925.

Baron AD, Brechtel G, Wallace P & Edelman SV (1988). Rates and tissue sites of non-insulin- and insulin-mediated glucose uptake in humans. *Am J Physiol Endocrinol Metab* **255**, E769–E774.

Brand MD (2000). Uncoupling to survive? The role of mitochondrial inefficiency in ageing. *Exp Gerontol* **35**, 811–820.

Brand MD (2005). The efficiency and plasticity of mitochondrial energy transduction. *Biochem Soc Trans* **33**, 897–904.

Brand MD & Nicholls DG (2011). Assessing mitochondrial dysfunction in cells. *Biochem J* **435**, 297–312.

Brown LD & Schneider MF (2002). Delayed dedifferentiation and retention of properties in dissociated adult skeletal muscle fibers in vitro. *In Vitro Cell Dev Biol Anim* **38**, 411–422.

Bruton JD, Dahlstedt AJ, Abbate F & Westerblad H (2003). Mitochondrial function in intact skeletal muscle fibres of creatine kinase deficient mice. *J Physiol* **552**, 393–402.

Bueschl C, Krska R, Kluger B & Schuhmacher R (2013). Isotopic labeling-assisted metabolomics using LC-MS. *Anal Bioanal Chem* **405**, 27–33.

Calderon JC, Bolanos P & Caputo C (2010). Myosin heavy chain isoform composition and Ca^{2+} transients in fibres from enzymatically dissociated murine soleus and extensor digitorum longus muscles. *J Physiol* **588**, 267–279.

Calderon JC, Bolanos P, Torres SH, Rodriguez-Arroyo G & Caputo C (2009). Different fibre populations distinguished by their calcium transient characteristics in enzymatically dissociated murine flexor digitorum brevis and soleus muscles. *J Muscle Res Cell Motil* **30**, 125–137.

Chen XL, Thorburn DR, Wong LJ, Vladutiu GD, Haas RH, Le T, Hoppel C, Sedensky M, Morgan P & Hahn SH (2011). Quality improvement of mitochondrial respiratory chain complex enzyme assays using *Caenorhabditis elegans. Genet Med* **13**, 794–799.

Chokkathukalam A, Kim DH, Barrett MP, Breitling R & Creek DJ (2014). Stable isotope-labeling studies in metabolomics: new insights into structure and dynamics of metabolic networks. *Bioanalysis* **6**, 511–524.

Ciammola A, Sassone J, Sciacco M, Mencacci NE, Ripolone M, Bizzi C, Colciago C, Moggio M, Parati G, Silani V & Malfatto G (2011). Low anaerobic threshold and increased skeletal muscle lactate production in subjects with Huntington's disease. *Mov Disord* **26**, 130–137.

Clark LC (1956). Monitor and control of blood and tissue oxygen tensions. *Trans Am Soc Artif Intern Organs* **2**, 41–48.

Clark LC & Sachs G (1968). Bioelectrodes for tissue metabolism. *Ann N Y Acad Sci* **148**, 133–153.

DeFronzo RA (1988). Lilly lecture 1987. The triumvirate: beta-cell, muscle, liver. A collusion responsible for NIDDM. *Diabetes* **37**, 667–687.

Drummond GB (2009). Reporting ethical matters in *The Journal of Physiology*: standards and advice. *J Physiol* **587**, 713–719.

Essen B, Jansson E, Henriksson J, Taylor AW & Saltin B (1975). Metabolic characteristics of fibre types in human skeletal muscle. *Acta Physiol Scand* **95**, 153–165.

Ferrick DA, Neilson A & Beeson C (2008). Advances in measuring cellular bioenergetics using extracellular flux. *Drug Discov Today* **13**, 268–274.

Fried NT, Moffat C, Seifert EL & Oshinsky ML (2014). Functional mitochondrial analysis in acute brain sections from adult rats reveals mitochondrial dysfunction in a rat model of migraine. *Am J Physiol Cell Physiol* **307**, C1017–C1030.

Gollnick PD, Riedy M, Quintinskie JJ & Bertocci LA (1985). Differences in metabolic potential of skeletal muscle fibres and their significance for metabolic control. *J Exp Biol* **115**, 191–199.

Gonzalez E, Messi ML, Zheng Z & Delbono O (2003). Insulin-like growth factor-1 prevents age-related decrease in specific force and intracellular Ca^{2+} in single intact muscle fibres from transgenic mice. *J Physiol* **552**, 833–844.

Grassi B, Poole DC, Richardson RS, Knight DR, Erickson BK & Wagner PD (1996). Muscle O_2 uptake kinetics in humans: Implications for metabolic control. *J Appl Physiol* **80**, 988–998.

Halseth AE, Bracy DP & Wasserman DH (2000). Limitations to basal and insulin-stimulated skeletal muscle glucose uptake in the high-fat-fed rat. *Am J Physiol Endocrinol Metab* **279**, E1064–E1071.

Huang L, Steyn FJ, Tan HY, Xie TY, Veldhuis JD, Ngo ST & Chen C (2012). The decline in pulsatile GH secretion throughout early adulthood in mice is exacerbated by dietary-induced weight gain. *Endocrinology* **153**, 4380–4388.

Hus-Citharel A & Morel F (1986). Coupling of metabolic CO_2 production to ion transport in isolated rat thick ascending limbs and collecting tubules. *Pflugers Arch* **407**, 421–427.

Isaeva EV, Shkryl VM & Shirokova N (2005). Mitochondrial redox state and Ca^{2+} sparks in permeabilized mammalian skeletal muscle. *J Physiol* **565**, 855–872.

Jung SK, Gorski W, Aspinwall CA, Kauri LM & Kennedy RT (1999). Oxygen microsensor and its application to single cells and mouse pancreatic islets. *Anal Chem* **71**, 3642–3649.

Koves TR, Ussher JR, Noland RC, Slentz D, Mosedale M, Ilkayeva O, Bain J, Stevens R, Dyck JR, Newgard CB, Lopaschuk GD & Muoio DM (2008). Mitochondrial overload and incomplete fatty acid oxidation contribute to skeletal muscle insulin resistance. *Cell Metab* **7**, 45–56.

Levine JA, Eberhardt NL & Jensen MD (1999). Role of nonexercise activity thermogenesis in resistance to fat gain in humans. *Science* **283**, 212–214.

Liesa M & Shirihai OS (2013). Mitochondrial dynamics in the regulation of nutrient utilization and energy expenditure. *Cell Metab* **17**, 491–506.

Mackrell JG & Cartee GD (2012). A novel method to measure glucose uptake and myosin heavy chain isoform expression of single fibers from rat skeletal muscle. *Diabetes* **61**, 995–1003.

Morino K, Petersen KF & Shulman GI (2006). Molecular mechanisms of insulin resistance in humans and their potential links with mitochondrial dysfunction. *Diabetes* **55**, S9–S15.

Palamiuc L, Schlagowski A, Ngo ST, Vernay A, Dirrig-Grosch S, Henriques A, Boutillier AL, Zoll J, Echaniz-Laguna A, Loeffler JP & Rene F (2015). A metabolic switch toward lipid use in glycolytic muscle is an early pathologic event in a mouse model of amyotrophic lateral sclerosis. *EMBO Mol Med* **7**, 526–546.

Pasarica M, Sereda OR, Redman LM, Albarado DC, Hymel DT, Roan LE, Rood JC, Burk DH & Smith SR (2009). Reduced adipose tissue oxygenation in human obesity evidence for rarefaction, macrophage chemotaxis, and inflammation without an angiogenic response. *Diabetes* **58**, 718–725.

Pearce JM, Pennington RJ & Walton JN (1964). Serum enzyme studies in muscle disease. II. serum creatine kinase activity in muscular dystrophy and in other myopathic and neuropathic disorders. *J Neurol Neurosurg Psychiatry* **27**, 96–99.

Pearson CM (1957). Serum enzymes in muscular dystrophy and certain other muscular and neuromuscular diseases. I. Serum glutamic oxalacetic transaminase. *N Engl J Med* **256**, 1069–1075.

Phielix E & Mensink M (2008). Type 2 diabetes mellitus and skeletal muscle metabolic function. *Physiol Behav* **94**, 252–258.

Picard M, Ritchie D, Wright KJ, Romestaing C, Thomas MM, Rowan SL, Taivassalo T & Hepple RT (2010). Mitochondrial functional impairment with aging is exaggerated in isolated mitochondria compared to permeabilized myofibers. *Aging Cell* **9**, 1032–1046.

Picard M, Taivassalo T, Ritchie D, Wright KJ, Thomas MM, Romestaing C & Hepple RT (2011). Mitochondrial structure and function are disrupted by standard isolation methods. *PLoS One* **6**, e18317.

Porter C, Hurren NM, Cotter MV, Bhattarai N, Reidy PT, Dillon EL, Durham WJ, Tuvdendorj D, Sheffield-Moore M, Volpi E, Sidossis LS, Rasmussen BB & Borsheim E (2015). Mitochondrial respiratory capacity and coupling control decline with age in human skeletal muscle. *Am J Physiol Endocrinol Metab* **309**, E224–E232.

Rogers GW, Brand MD, Petrosyan S, Ashok D, Elorza AA, Ferrick DA & Murphy AN (2011). High throughput microplate respiratory measurements using minimal quantities of isolated mitochondria. *PLoS One* **6**, e21746.

Rolfe DF & Brand MD (1996). Contribution of mitochondrial proton leak to skeletal muscle respiration and to standard metabolic rate. *Am J Physiol Cell Physiol* **271**, C1380–C1389.

Rolfe DF, Newman JM, Buckingham JA, Clark MG & Brand MD (1999). Contribution of mitochondrial proton leak to respiration rate in working skeletal muscle and liver and to SMR. *Am J Physiol Cell Physiol* **276**, C692–C699.

Rossi AE, Boncompagni S, Wei L, Protasi F & Dirksen RT (2011). Differential impact of mitochondrial positioning on mitochondrial Ca^{2+} uptake and Ca^{2+} spark suppression in skeletal muscle. *Am J Physiol Cell Physiol* **301**, C1128–1139.

Schiaffino S & Reggiani C (2011). Fiber types in mammalian skeletal muscles. *Physiol Rev* **91**, 1447–1531.

Schuh RA, Jackson KC, Khairallah RJ, Ward CW & Spangenburg EE (2012). Measuring mitochondrial respiration in intact single muscle fibers. *Am J Physiol Regul Integr Comp Physiol* **302**, R712–R719.

Schuh RA, Jackson KC, Schlappal AE, Spangenburg EE, Ward CW, Park JH, Dugger N, Shi GL & Fishman PS (2014). Mitochondrial oxygen consumption deficits in skeletal muscle isolated from an Alzheimer's disease-relevant murine model. *BMC Neurosci* **15**, 24.

Selvin D, Hesse E & Renaud JM (2015). Properties of single FDB fibers following a collagenase digestion for studying contractility, fatigue, and pCa-sarcomere shortening relationship. *Am J Physiol Regul Integr Comp Physiol* **308**, R467–R479.

Shan G, Huang W, Gee SJ, Buchholz BA, Vogel JS & Hammock BD (2000). Isotope-labeled immunoassays without radiation waste. *Proc Natl Acad Sci USA* **97**, 2445–2449.

Simoneau JA, Veerkamp JH, Turcotte LP & Kelley DE (1999). Markers of capacity to utilize fatty acids in human skeletal muscle: relation to insulin resistance and obesity and effects of weight loss. *FASEB J* **13**, 2051–2060.

Sparks LM, Xie H, Koza RA, Mynatt R, Hulver MW, Bray GA & Smith SR (2005). A high-fat diet coordinately downregulates genes required for mitochondrial oxidative phosphorylation in skeletal muscle. *Diabetes* **54**, 1926–1933.

Spinazzi M, Casarin A, Pertegato V, Salviati L & Angelini C (2012). Assessment of mitochondrial respiratory chain enzymatic activities on tissues and cultured cells. *Nat Protoc* **7**, 1235–1246.

Stackley KD, Beeson CC, Rahn JJ & Chan SSL (2011). Bioenergetic profiling of zebrafish embryonic development. *PLoS One* **6**, e25652.

Steyn FJ, Xie TY, Huang L, Ngo ST, Veldhuis JD, Waters MJ & Chen C (2013). Increased adiposity and insulin correlates with the progressive suppression of pulsatile GH secretion during weight gain. *J Endocrinol* **218**, 233–244.

Stout MB, Steyn FJ, Jurczak MJ, Camporez JG, Zhu Y, Hawse JR, Jurk D, Palmer AK, Xu M, Pirtskhalava T, Evans GL, de Souza Santos R, Frank AP, White TA, Monroe DG, Singh RJ, Casaclang-Verzosa G, Miller JD, Clegg DJ, LeBrasseur NK, von Zglinicki T, Shulman GI, Tchkonia T & Kirkland JL (2016). 17α-Estradiol alleviates age-related metabolic and inflammatory dysfunction in male mice without inducing feminization. *J Gerontol A Biol Sci Med Sci* (in press; doi: 10.1093/gerona/glv309).

Suarez RK, Brown GS & Hochachka PW (1986). Metabolic sources of energy for hummingbird flight. *Am J Physiol Regul Integr Comp Physiol* **251**, R537–R542.

Suga T, Kinugawa S, Takada S, Kadoguchi T, Fukushima A, Homma T, Masaki Y, Furihata T, Takahashi M, Sobirin MA, Ono T, Hirabayashi K, Yokota T, Tanaka S, Okita K & Tsutsui H (2014). Combination of exercise training and diet restriction normalizes limited exercise capacity and impaired skeletal muscle function in diet-induced diabetic mice. *Endocrinology* **155**, 68–80.

Talan M (1984). Body temperature of C57BL/6J mice with age. *Exp Gerontol* **19**, 25–29.

Thorburn DR (2000). Practical problems in detecting abnormal mitochondrial function and genomes. *Hum Reprod* **15 Suppl 2,** 57–67.

To MS, Aromataris EC, Castro J, Roberts ML, Barritt GJ & Rychkov GY (2010). Mitochondrial uncoupler FCCP activates proton conductance but does not block store-operated Ca^{2+} current in liver cells. *Arch Biochem Biophys* **495**, 152–158.

Tricarico D, Mele A, Lundquist AL, Desai RR, George AL Jr & Conte Camerino D (2006). Hybrid assemblies of ATP-sensitive K^+ channels determine their muscle-type-dependent biophysical and pharmacological properties. *Proc Natl Acad Sci USA* **103**, 1118–1123.

Van Bergen NJ, Blake RE, Crowston JG & Trounce IA (2014). Oxidative phosphorylation measurement in cell lines and tissues. *Mitochondrion* **15**, 24–33.

Weis-Fogh T (1967). Metabolism and weight economy in migrating animals, particularly birds and insects. In *Insects and Physiology*, ed. Beament JWL & Treherne JE, pp. 143–159. Oliver & Boyd, Edinburgh.

Wells GD, Noseworthy MD, Hamilton J, Tarnopolski M & Tein I (2008). Skeletal muscle metabolic dysfunction in obesity and metabolic syndrome. *Can J Neurol Sci* **35**, 31–40.

Westerblad H, Bruton JD & Lannergren J (1997). The effect of intracellular pH on contractile function of intact, single fibres of mouse muscle declines with increasing temperature. *J Physiol* **500**, 193–204.

Wu M, Neilson A, Swift AL, Moran R, Tamagnine J, Parslow D, Armistead S, Lemire K, Orrell J, Teich J, Chomicz S & Ferrick DA (2007). Multiparameter metabolic analysis reveals a close link between attenuated mitochondrial bioenergetic function and enhanced glycolysis dependency in human tumor cells. *Am J Physiol Cell Physiol* **292**, C125–C136.

Zhang J, Nuebel E, Wisidagama DRR, Setoguchi K, Hong JS, Van Horn CM, Imam SS, Vergnes L, Malone CS, Koehler CM & Teitell MA (2012*a*). Measuring energy metabolism in cultured cells, including human pluripotent stem cells and differentiated cells. *Nat Protoc* **7**, 1068–1085.

Zhang Y, Huang JJ, Wang ZQ, Wang N & Wu ZY (2012*b*). Value of muscle enzyme measurement in evaluating different neuromuscular diseases. *Clin Chim Acta* **413**, 520–524.

Zurlo F, Larson K, Bogardus C & Ravussin E (1990). Skeletal-muscle metabolism is a major determinant of resting energy-expenditure. *J Clin Invest* **86**, 1423–1427.

Additional information

Competing interests

The authors declare that they have no competing interests.

Author contributions

Experiments were performed in the Integrated Physiology Facility (IPF) and S.T.N.'s laboratory at the School of Biomedical Sciences, University of Queensland. R.L. optimised and performed the bioenergetics experiments, analysed and interpreted data, and drafted and revised the manuscript. F.J.S. and M.B.S. designed and conducted the high-fat feeding experiments, analysed and interpreted the data, and revised the manuscript. K.L. assisted with animal dissection and revised the manuscript. T.R.C. assisted in optimising the muscle fibre isolation procedure and revised the manuscript. J.C.C. provided critical intellectual input for the isolation of muscle fibres and revised the manuscript. S.T.N. conceived and designed the study, interpreted data and critically revised the manuscript. All authors approve the final version of the manuscript and agree to be accountable for all aspects of the work in ensuring that questions related to the accuracy or integrity of any part of the work are appropriately investigated and resolved. All persons designated as authors qualify or authorship, and all those who qualify for authorship are listed.

Funding

This work was funded by start-up support from the School of Biomedical Sciences at the University of Queensland, and a Motor Neurone Disease Research Institute of Australia (MNDRIA) Bob Delaney MND Research Grant to S.T.N. R.L. is the recipient of an international postgraduate research scholarship from the Australian Government, and a University of Queensland centennial scholarship. S.T.N. is the Scott Sullivan MND Research Fellow and is funded by the Queensland Brain Institute, the Royal Brisbane and Women's Hospital Foundation, and The MND and Me Foundation.

Acknowledgements

The authors gratefully acknowledge the assistance and support of staff at the University of Queensland Biological Resources (UQBR).